International Journal of Refrigeration 180 (2025) 535–547

Contents lists available at ScienceDirect

International Journal of Refrigeration

journal homepage: www.elsevier.com/locate/ijrefrig

INSTITUT INTERNATIONAL DU FROID
INTERNATIONAL INSTITUTE OF REFRIGERATION

Performance evaluation of R744-hydrocarbon blends in a two-stage refrigeration cycle for transport applications

William Ferretto *, Chiara D'Ignazi, Igor Matteo Carraretto, Luca Molinaroli

Dipartimento di Energia, Politecnico di Milano, Via Lambruschini 4, 20156, Milano, Italy

ARTICLE INFO

Keywords:
Binary mixtures
Carbon dioxide
Hydrocarbons
Performance assessment
Refrigerated transport

ABSTRACT

The increasing environmental concerns and regulations are forcing the HVAC&R sector to shift towards low-GWP refrigerants. Hence, research is actively exploring sustainable alternatives to traditional HFC-based systems. This study provides a numerical drop-in analysis of CO_2 (R744) - hydrocarbon blends in a two-stage vapor compression cycle designed for a mid-sized refrigerated truck. By simulating blends of R744 with small amounts (up to 10 %) of R290, R600a, R1270, and RE170 under various ambient conditions, this research identifies the options that could match or enhance the performance with respect to pure R744. Seasonal simulations, accounting for typical thermal loads in two Italian cities, i.e., Milan and Palermo, reveal that R744 blends with R290 and R1270 achieve comparable or improved seasonal COP (SCOP), especially in colder climates where the system performance benefits from temperature glide. The optimal blend, 92 % R744 and 8 % R290, provides SCOP increases of 2.96 % in Milan and 2.13 % in Palermo, while blends with R600a or RE170 show reduced efficiency. These findings suggest the R744 - R290 and R744 - R1270 blends as a promising low-GWP option for refrigerated transport.

1. Introduction

Refrigerated transport is crucial in the supply chains of various industries, particularly in the food and pharmaceutical sectors, as it enables the safe transportation of goods that require temperature-controlled environments. According to European market projections (IMARC, 2023), this sector is expected to grow by 4 % per year up to 2050. Most vehicles in this sector rely on vapor compression systems, operated with Hydro-Fluoro-Carbons (HFC) refrigerants, which are characterized by a high Global Warming Potential (GWP). Regulations like (EU, 2024) envisage a gradual phase-out of high-GWP refrigerants, pushing the industry towards natural alternatives with a lower environmental impact. As highlighted in the review by Minetto et al. (2023), R744 (CO_2) has emerged as a promising natural refrigerant for this sector, being both non-toxic and non-flammable, and having both a zero Ozone Depletion Potential (ODP) and a GWP of 1.

Several studies have focused on the simulation of refrigeration vehicles with R744-based vapor compression cycles operated with different system configurations. In their study, Artuso et al. (2020) conducted a theoretical evaluation of a R744 vapor compression system designed for refrigerated transport, focusing on three distinct configurations: a standard layout with a low-pressure receiver and two different setups that incorporated a two-phase ejector, one of which also included an auxiliary evaporator. They found that the adoption of an ejector is more advantageous in hot climates, with a maximum benefit of approximately 16 % at an ambient temperature of 42 w°C. In an analogous study, Fabris et al. (2021) analyzed the same three configurations previously mentioned through dynamic simulations, modeling a typical long-distance delivery scenario in Athens in August. In their study they showed that the adoption of an ejector improves mostly the system's performance at high environmental temperatures, confirming their previous findings. Eventually, Fabris et al. (2024) performed a numerical analysis of a R744 vapor compression system operating at two different evaporation levels. They compared a simple configuration with an ejector cycle, demonstrating that the ejector configuration has a higher COP but the standard system provides greater flexibility in cooling capacity production.

Previously mentioned studies have demonstrated that vapor compression systems operating with R744 require higher technical complexity, including components such as the above-mentioned ejectors or multi-level pressure configurations. These enhancements are mandatory to address the inherent inefficiencies of the transcritical vapor compression cycle (Kim, 2004), often employed due to the low critical temperature of R744 (i.e., 30.98 °C). Moreover, R744 has a high critical pressure (i.e., 7380 kPa) which leads to high operating pressures, increasing consequently the constraints on the mechanical design of system. To overcome these issues and enhance performance, researchers are currently

* Corresponding author.
E-mail address: william.ferretto@polimi.it (W. Ferretto).

https://doi.org/10.1016/j.ijrefrig.2025.09.024
Received 26 May 2025; Received in revised form 17 September 2025; Accepted 21 September 2025
Available online 24 September 2025

Nomenclature

Acronyms

HP	High Pressure
HX	Heat Exchanger
LP	Low pressure
NTU	Number of transfer units
a	Absorptivity –
c_p	Specific heat at constant pressure $J\,K^{-1}\,kg^{-1}$
e	Emissivity –
f	Inverter frequency Hz
G	Irradiance $W\,m^{-2}$
h	Enthalpy $J\,kg^{-1}$
k	Thermal conductivity $W\,m^{-1}\,K^{-1}$
L_C	Characteristic length m
M	Molar mass $g\,mol^{-1}$
$\dot{m}$	Mass flow rate $kg\,s^{-1}$
n	Number of air volume changes per hour h^{-1}
Nu	Nusselt number –
p	Pressure Pa
$\dot{Q}$	Heat transfer rate W
RPM	Rotations per minute rpm
RH	Relative humidity %
s	Thickness m
T	Temperature K
ΔT	Temperature difference K
V	Volume m^3
$\dot{V}$	Volumetric flow rate $m^3\,s^{-1}$
$\dot{W}$	Mechanical power W
V_D	Compressor displacement m^3
x	Vapor quality –
y	Mass fraction of secondary fluid in mixture–

Greek symbols

α	Convective heat transfer coefficent $W\,m^{-2}\,K^{-1}$
β	Pressure ratio –
ε	Heat exchanger effectiveness –
η	Efficiency –
θ	Solar altitude angle rad
ρ	Density $kg\,m^{-3}$
σ	Stefan-Boltzmann constant $W\,m^{-2}\,K^{-4}$

Subscripts

AIR	Air
C	Cooling
COMP	Compressor
CRIT	Critical
CV	Convection
EVA	Evaporator
EXT	External
FC	Forced convection
FT	Flash tank
HP	High pressure
IN	Inlet
INS	Insulation material
INT	Internal
IRR	Radiative
K	Conduction
MIN	Minimum
NC	Natural convection
OUT	Outlet
REF	Refrigerant
S	Isentropic
SAT	Saturation
SH	Superheat
SKY	Sky
V	Saturated vapor
VOL	Volumetric
W	Wall

exploring the potential of R744-based blends and exploit their tailored thermo-physical properties. First, the temperature glide, which appears during phase change phenomena, can be leveraged to optimize the system performance. Specifically, it allows the refrigerant to better follow the temperature profile of the secondary fluid, consequently minimizing the heat transfer losses (Cao et al., 2017). Secondly, the working fluid's critical pressure can be decreased, enabling operation in subcritical mode at higher ambient temperatures and reducing the operating pressure, which, in turn, leads to a reduction of the system weight, cost and control complexity.

On this topic, major effort is put on the analysis of R744 blends with hydrocarbons (HCs), thanks to their low environmental impact (0 ODP, low GWP, PFAS-free) and suited thermo-physical properties (high critical temperature, low critical pressure). However, they have high flammability, which consistently reduces their applicability as standalone fluids in large capacity systems. Most of the research on the subject has focused on the performance of traditional systems configurations operated with this innovative blends, mainly made by small quantities of HC in order to limit the fluid flammability. Tobaly et al. (2018) experimentally evaluated the use of R744-propane blends (5 %, 10 % and 15 % molar R290) in a refrigeration system equipped with an Internal Heat Exchanger (IHX). The study showed that the operating pressure is consistently reduced, with variations ranging approximately from -5.5 % to -21.5 %, depending on the propane concentration and the operating conditions. Additionally, the COP can be increased by up to 20 %.

Sánchez et al. (2024) experimentally studied mixtures of R744 with R32, R1270, and R1234yf in a transcritical refrigeration system in a drop-in analysis and evaluated the presence of the IHX in the system. The results show a COP improvement of up to 15.3 % with R744/R32 compared to R744 without IHX, and a COP improvement up to 22 % with R744/R32 compared to R744 with IHX. Furthermore, each R744-based mixture studied exhibited a reduction in heat rejection pressure, ranging from 250 to 1620 kPa, with no significant differences between configurations with or without the IHX. Sánchez et al. (2019), also showed that a reduction in energy consumption of up to 10.3 % can be achieved by using a mixture of R744/R1270 (91/9 %w) instead of pure R744 in a beverage cooler system.

From a modeling perspective, Xie et al. (2021) developed a numerical investigation of R744 mixtures to enhance the performance of pure R744 in a trans-critical refrigeration system. The results show that the optimized mixtures of R744/R152a (0.875/0.125) and R744/R161 (0.85/0.15) can achieve a COP improvement of about 30 % with a reduction in discharge pressure compared to R744 of 1600 kPa and 1800 kPa, respectively. Moreover, Vaccaro et al. (2023) modeled various R744 blends and concluded that R744/R1234yf offered the best COP improvement, while R744/propane blends also showed performance enhancements and lower gas cooler pressures. Eventually, Sánchez et al. (2023) further investigated R744-based blends with a focus on refrigerants with GWP values below 150 and non-flammability criteria. Their research identified R744/R32 (81/19 % by mass) and R744/R1270 (92.5/7.5 % by mass) as the most promising options for new systems, achieving COP improvements of 21.39 % and 8.66 %, respectively. When blending R744 with hydrocarbons, flammability becomes a key consideration. Several studies have aimed to establish criteria for classifying the

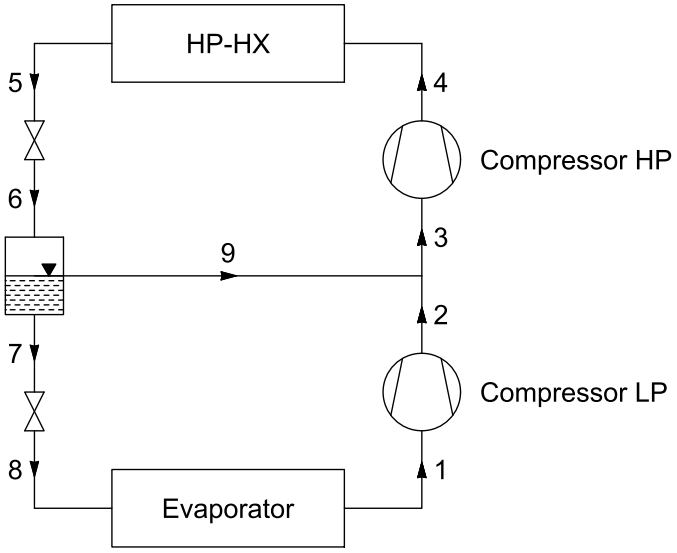

Fig. 1. Plant layout.

flammability of such mixtures. Kondo et al. (2006) extended Le Chatelier's formula to show that the flammability limits of various compounds can be described using common parameters. Linteris et al. (2019) proposed the evaluation of the adiabatic flame temperature and fluorine substitution ratio, introducing a flammability index (Π) to capture both variables and distinguish between A1 and A2L refrigerants. Calleja-Anta et al. (2022) later applied this approach to define the A2-A3 boundary, finding that mixtures exceeding a 67.37° flammability index fall under the A3 classification. They used this methodology to identify hydrocarbon blends that meet A2 safety standards with a GWP below 150.
Despite an increasing number of studies have been carried out in last years, the knowledge on the topic is still limited both from experimental and numerical point of view. On the latter, most of the analysis focus on system design in a single operating point rather than a drop-in analysis on seasonal perspective, which may lead to inappropriate conclusions.

This research aims at numerically investigate the performance of R744-hydrocarbon blends for refrigerated transport applications and compare it against that of a pure R744 cycle. Specifically, this work presents a drop-in analysis of different mixtures in a two-stage vapor compression cycle designed for pure R744. Blends of R744 and alternatively propane (R290), isobutane (R600a), propylene (R270) and dimethyl-ether (RE170) at different concentrations are considered. The simulations are performed using a semi-analytical model, with each component modeled separately through specific sub-model, then integrated into the simulation structure. Both heat exchangers are simulated using an analytical approach, allowing for a detailed description of the heat transfer process in such particular mixtures, representing an advancement over previous studies. A mid-sized refrigerated truck is used as a reference for cooling load computations. The cycle operating parameters are optimized for each ambient temperature over a typical year of two Italian cities, i.e., Milan and Palermo. Ultimately, the seasonal coefficient of performance is the quantity used to compare the performance of the various fluids.

2. Refrigeration system

Fig. 1 shows the layout of the simulated refrigeration cycle, which consists of an air to air two-stage compression plant.

The main components of the refrigerant loop are:

- A fixed speed semi-hermetic reciprocating low pressure (LP) compressor (1–2).
- A variable speed semi-hermetic reciprocating high pressure (HP) compressor (3–4).
- A fin-and-tube heat exchanger (high pressure heat exchanger (HP-HX)) (4–5).
- A high pressure electronic expansion valve (5–6).
- A flash tank (6–7).
- A low pressure electronic expansion valve (7–8).
- A fin-and-tube heat exchanger (evaporator) (8-1).

It has to be noted that the HP-HX can act as a condenser, when the operating pressure is below the critical pressure, or as a gas cooler, when the operating pressure is above the critical pressure.

2.1. Refrigeration system model

In this work, a semi-analytical model able to simulate the steady-state operations of the refrigeration system is developed. Each component is modeled individually through specific sub-models, and then integrated into the simulation structure of an in-house developed algorithm.

2.1.1. Heat exchangers

The models adopted for both heat exchangers were previously developed and validated by the authors against experimental data Joppolo et al. (2015) and Ferretto et al. (2025), showing satisfactory agreement. They have been suitably modified to account for different fluids and operating conditions, as reported below. The fin-and-tube heat exchangers are modeled according to the elemental volume approach. Each heat exchanger is subdivided into a series of elemental volumes, which are sufficiently small to provide good computational accuracy (discrepancy error between air and refrigerant energy balances lower than 0.1 %). The following assumptions are made:

- Negligible superheated condensation.
- Negligible subcooled boiling.
- Negligible kinetic and potential energy.
- Adiabatic tube bends.

Mass, momentum and energy equations are solved inside each elemental volume, which is composed of a refrigerant stream, tube, fins, and air stream, as shown in Fig. 2.

The volume is treated as a cross-flow heat exchanger, with the air stream identified as the unmixed stream and the refrigerant stream as the mixed one. The heat transfer $\dot{Q}(i)$ is computed through the ε-NTU method:

$$\dot{Q}(i) = \varepsilon(i) \cdot (\dot{m}c_p)_{MIN,i} \cdot \left(T_{REF}(i) - T_{AIR}(i)\right) \quad (1)$$

$$\dot{Q}(i) = \dot{m}_{REF}(i) \cdot \left(h_{REF}(i+1) - h_{REF}(i)\right) \quad (2)$$

$$\dot{Q}(i) = \dot{m}_{AIR}(i) \cdot \left(h_{AIR}(i) - h_{AIR}(i+1)\right) \quad (3)$$

Eqs. (1)–(3) are solved to provide the heat transfer on a generic elemental volume *i*. The heat exchange effectiveness ε is provided by specific formulation reported in ESDU (2014). The correlations used for the description of heat transfer and pressure drop of both refrigerant and airare reported in Table 1. The heat transfer correlations are not used directly with mixtures but are modified using the well-established correction proposed by Bell and Ghaly (1972) which relates the temperature glide of the mixture to a penalization in both condensation and evaporation, whereas for pressure drop the influence of the mixture was not considered as there is no established procedure in literature for these mixtures. On the air side, the flow rate is computed through the fluid-dynamic match between the heat exchanger and the corresponding fan. For simplicity, frost and dehumidification on the evaporator are not considered.

2.1.2. Compressor

LP and HP compressors are sized according to the mass flow rate requested to satisfy the design cooling load. The main characteristic are

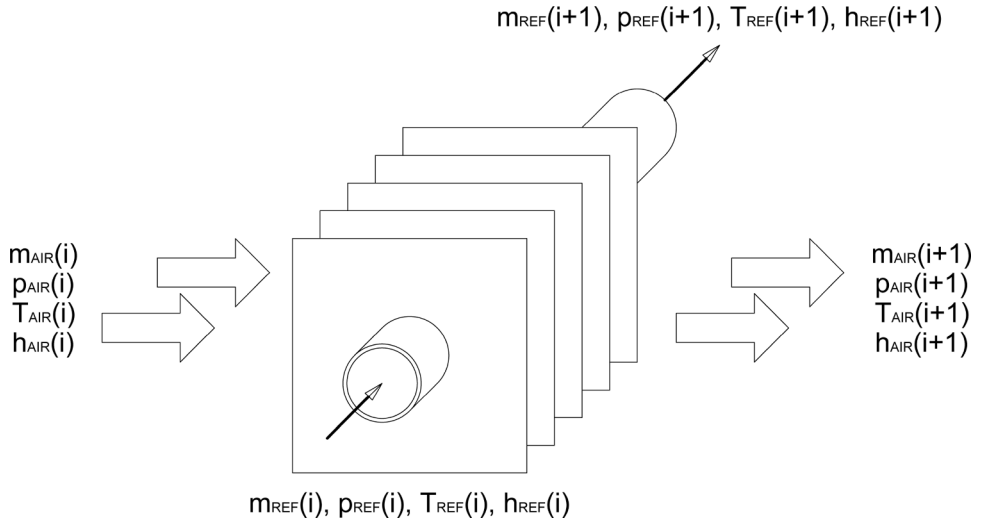

Fig. 2. Schematic of a generic elemental volume.

Table 1
Refrigerant and air-side heat-transfer and pressure-drop correlations.

	Single phase		Two-phase		Air
	Sub-critical	Trans-critical	Condensation	Evaporation	
Heat transfer	Gnielinski (1976)	Pitla et al. (2002)	Cavallini et al. (2006)	Kim and Mudawar (2013)	Wang et al. (1999)
Pressure drop	Blasius (1913)	Blasius (1913)	Kim and Mudawar (2012)	Zhang and Webb (2001)	Wang et al. (1999)

retrieved from a pure R744 selection software, which provides also isentropic and volumetric efficiency. The following equations are used to model the two compressors:

$$\dot{m}_{REF,COMP} = \rho_{IN} \cdot \eta_{VOL} \cdot V_D \cdot \frac{RPM}{60} \tag{4}$$

$$\dot{W}_{COMP} = \dot{m}_{REF,COMP} \cdot \frac{h_{OUT,S} - h_{IN}}{\eta_S} \tag{5}$$

Note that the compressor rotational speed is fixed for the LP compressor, whereas it changes according to the inverter frequency in the HP compressor.
The volumetric and isentropic efficiencies (η_{VOL} and η_S) are modeled through the following equations:

$$\eta_{VOL} = b_0 + b_1 \cdot \Delta T_{SH} + b_2 \cdot \beta \tag{6}$$

$$\eta_S = c_0 + c_1 \cdot \Delta T_{SH} + c_2 \cdot \exp(c_3 \cdot \beta) + c_4 \cdot \exp(c_5 \cdot \beta) \tag{7}$$

The selection software of a manufacturer is employed to fit η_v and η_s. Specifically, several T_{evap} and T_{cond} are considered to compute $\dot{m}$ and $\dot{W}$ under reference conditions. Subsequently, the Dabiri and Rice (1981) correction is applied to account for deviations of the superheat from the reference value. Finally, both efficiencies are expressed as functions of the compressor superheat and pressure ratio. The residual minimization procedure indicates that the best-fitting model for the volumetric efficiency is linear with pressure ratio and superheat, whereas the isentropic efficiency is best described by a linear dependence on superheat and an exponential one on pressure ratio. The resulting models, shown in Eqs. (6) and (7), which include the best fit coefficients $b_0 - b_2$ and $c_0 - c_5$, are subsequently used in Eqs. (4) and (5) to compute the required quantities for all different fluids. It has to be noted that limited data on isentropic and volumetric efficiencies is available in open literature for compressors operating with R744-HCs mixtures. Therefore, the coefficients are fitted on pure R744 data and used for R744-HCs mixtures, which is acknowledged as a limitation of this work. The inverter frequency of the HP compressor is adjusted to suck the refrigerant flow rate coming from the LP compressor and that at the outlet of the flash tank according to:

$$f_{COMP} = \frac{\dot{m}_{REF,3}}{\dot{m}_{COMP,50}} \cdot 50\ [Hz] \tag{8}$$

The rotational frequency f_{COMP} can vary between 30–70 Hz. In the system simulations, the frequency is free to vary outside the operative range while the analysis of the results consider only simulation data in which the frequency stays in the 30–70 Hz range.

2.1.3. Flash tank and expansion valves

The optimization of flash tank pressure aims at maximizing COP. Although a COP-capacity trade-off may be relevant in applications like refrigerated trucks, this study focuses on energy efficiency with the final target of reducing the overall energy consumption and environmental impact of the truck. Once the flash tank pressure is set, the refrigerant quality and temperature are computed as function of both pressure and enthalpy, which are evaluated at the HP-HX outlet. Then, the composition of both liquid and vapor streams is computed, capturing the composition shift through the flash tank. The mass flow rate of vapor and liquid are computed and fed to the corresponding nodes as reported in Fig. 1. The following equations summarize the flash tank resolution. First, the saturation temperature at which the flash tank operates T_{FT} is computed provided the operating pressure p_{FT} and the enthalpy at the outlet of the high-pressure heat exchanger $h_{HP,OUT}$:

$$T_{FT} = T(p_{FT}, h_{HP,OUT}) \tag{9}$$

then, the compositions of the liquid (7) and vapor (9) streams are computed as the bubble and dew compositions at the operating conditions of the flash tank respectively:

$$\begin{cases} y_7 = y(p_{FT}, T_{FT}, x_7 = 0) \\ y_9 = y(p_{FT}, T_{FT}, x_9 = 1) \end{cases} \tag{10}$$

finally, the liquid and vapor mass flow rates are computed according to the vapor quality at the outlet of the back-pressure valve:

$$\begin{cases} \dot{m}_{REF,7} = (1 - x_6) \cdot \dot{m}_{REF,6} \\ \dot{m}_{REF,9} = x_6 \cdot \dot{m}_{REF,6} \end{cases} \tag{11}$$

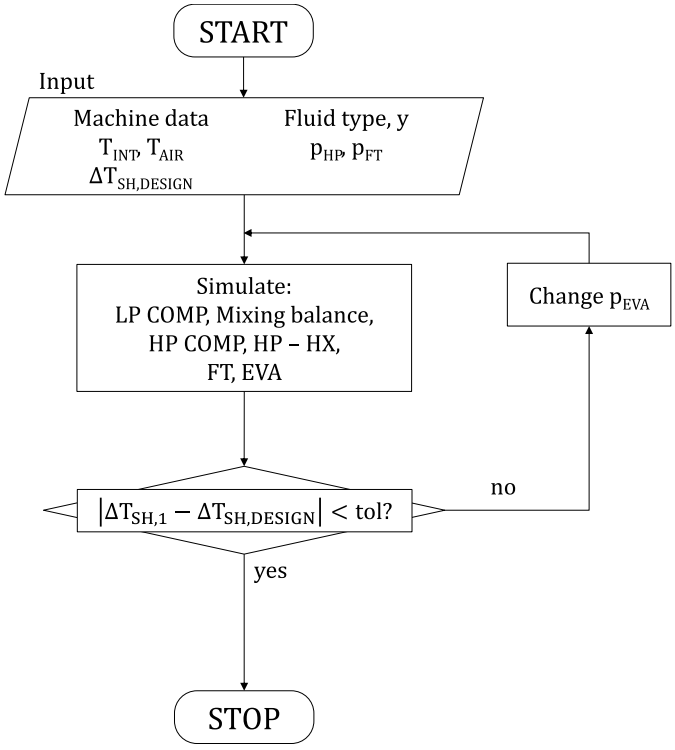

Fig. 3. Machine resolution algorithm.

Eventually, the expansion valves are assumed to be adiabatic, hence the processes 5–6 and 7–8 in Fig. 1 are isenthalpic.

2.1.4. Resolution algorithm

The components previously described are simulated together according to the resolution algorithm, shown in Fig. 3. The simulation is initialized and fed with the required data, including heat exchanger geometry and parameters, compressor and fan characteristic curves, then, it starts from the inlet of LP compressor, and all the components till the evaporator outlet are solved sequentially. Subsequently, the LP compressor superheat is compared with the required superheat $\Delta T_{SH,DESIGN}$, set to 5 K. If the two are different, evaporating pressure is adjusted and the whole cycle is simulated from the beginning. Specifically, p_{EVA} is increased to reduce the simulated superheat, or *viceversa* decreased to increase the simulated superheat. Eventually, the bisection method is used to reach the desired value.

2.2. Simulation space

The plant is simulated changing the following variables:

- Working fluids.
- Blend compositions.
- Flash tank pressure.
- HP-HX pressure.
- HP-HX inlet air temperatures.

2.2.1. Working fluids

As reported in the Introduction, binary mixtures of R744 with R290 or R600a or R1270 or R-E170 (DME) are considered. The main properties of the 5 refrigerants are shown in Table 2. It can be highlighted that the three HCs and the ether have all good environmental characteristics (low GWP and low toxicity), a lower critical pressure, a higher critical temperature and a significantly lower density with respect to pure CO_2. Hence, owing to the volumetric nature of the compressor, the mass flow rate will be reduced with respect to the reference case (i.e., pure R744).

Table 2
Refrigerants properties (Safety Code and GWP_{100} according to UNI (2021)).

Refrigerant	M [g mol^{-1}]	p_{CRIT} [kPa]	T_{CRIT} [°C]	ρ_V(@ −25°C) [kg m^{-3}]	Safety Code	GWP_{100}
R744	44.01	7380	31.10	43.88	A1	1
R290	44.10	4250	96.70	4.63	A3	3
R600a	58.12	3640	134.70	1.69	A3	3
R1270	42.08	4670	92.40	5.59	A3	2
RE170	46.07	5337	127.23	2.33	A3	1

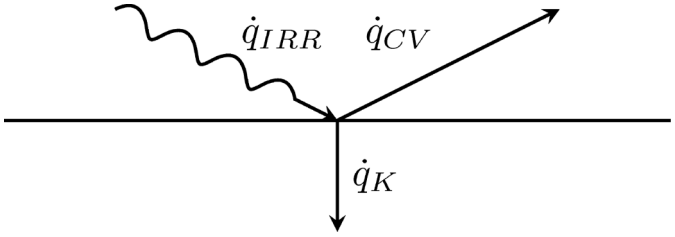

Fig. 4. Energy balance on the surface of the tuck envelope.

In this work, the fluid properties are evaluated using REFPROP v. 10.0 (Lemmon et al., 2018), with default interaction parameters for mixtures characterization.
According to Calleja-Anta et al. (2022), the nominal composition limits required to ensure an A2 safety classification are as follows: R290/R744 at 4.6 %/95.4 %, R600a/R744 at 0.9 %/99.1 %, and R1270/R744 at 4.2 %/95.8 % by mass. No corresponding composition is provided for RE170/R744 mixture.

2.2.2. Other variables and simulation ranges

Concerning the fluid composition, 6 equally spaced points are considered, i.e., y = 0 % (pure R744), 2 %, 4 %, 6 %, 8 % and 10 %. Flash tank pressure p_{FT} and and HP heat exchanger pressure p_{HP} are optimized according to the operating temperature. Specifically, as explained before, p_{HP} could represent a subcritical or a transcritical pressure according to the best performing operating condition at each ambient temperature.

The ambient air temperature T_{AIR} ranges from 0 to 40 °C, which is a sufficiently large range to include the temperature distribution of the chosen locations across a year.

2.3. Thermal loss

The thermal loss of the truck, i.e., the capacity the refrigeration system has to compensate for, is computed through an energy balance at truck envelope surface, as shown in Fig. 4.

On each surface, the energy balance is the combination of three different contributions, namely conductive, convective and radiative:

$$\dot{q}_K + \dot{q}_{CV} = \dot{q}_{IRR} \tag{12}$$

It is assumed that the external surfaces are plane walls. The front wall, which is typically covered by the cabin, is considered adiabatic. The insulation material is considered to be isotropic and uniform, and the three dimensional effects on conduction are considered negligible. Hence, the conductive heat flux is computed as follows:

$$\dot{q}_K = \frac{T_i - T_W}{\frac{s_{INS}}{k_{INS}}} = \frac{T_i - T_{INT}}{\frac{s_{INS}}{k_{INS}}} \tag{13}$$

It is assumed that the interior fans provide a very high heat transfer convective coefficient, hence the temperature of surfaces inside the refrigerated truck T_W is set at the temperature of the cooled air. The convective heat flux is computed through the Newton's law:

$$\dot{q}_{CV} = \alpha_{CV} \cdot (T_i - T_{EXT}) \tag{14}$$

Table 3
Insulation material thickness.

Side	Thickness [mm]
Roof	105
Floor	100
Rear	70
Front	105
Side	45

The heat transfer coefficient is computed according to plane wall correlations (Incropera et al., 2006) for both natural and forced convection, which are then combined according to the following equation:

$$\alpha_{CV} = \frac{k_{AIR}}{L_C} \cdot \sqrt[3.2]{Nu_{FC}^{3.2} + Nu_{NC}^{3.2}} \tag{15}$$

If the truck is moving, it is assumed that the air velocity is the truck velocity.
The net radiative heat flux, is composed of the solar irradiation and the radiative emission from the surface to the sky, and is computed as follows:

$$\dot{q}_{IRR} = G \cdot a \cdot \begin{cases} \sin\theta & \text{for horizontal wall} \\ \cos\theta & \text{for vertical wall} \end{cases} - e \cdot \sigma \cdot (T_i^4 - T_{SKY}^4) \tag{16}$$

The incoming radiation is considered only in its normal component through the solar altitude angle θ, computed according to Reda and Andreas (2008). It is assumed that the truck is always perfectly oriented with the solar azimuth. Absorbed radiation is neglected on the tailgate wall while the total radiative heat flux is zero for the floor wall. The sky temperature is computed according to Berdahl and Martin (1984), assuming a constant relative humidity of 50 %.
Lastly, a heat loss representative of door openings is added as follows:

$$\dot{Q}_D = \rho_{AIR}(T_{INT}) \cdot V_{INT} \cdot n \cdot \Big[h_{AIR}(T_{EXT}, RH_{EXT}) - h_{AIR}(T_{INT}, RH_{INT}) \Big] \tag{17}$$

The relative humidity of internal and external air is considered to be 50 %, and the number of air volume changes n is set at 1 [1/h]. Although no specific reference was found, it is believed to be realistic that a mid-sized refrigerated truck could open the door once every hour for enough time to change the air volume of the truck. For simplicity, it is assumed that the view factor between the side and rear walls and the ground is zero.

3. Case study description

3.1. Refrigerated truck

As stated in the Introduction, the present work aims at the steady state simulation of a refrigerated truck with different fluids, hence, a reference mid-size truck is considered. The truck internal volume is 19.73 m^3 (4020 mm x 2394 mm x 2050 mm) and it is insulated by XPS panels with different thickness, as reported in Table 3. The XPS thermal conductivity is assumed to be 0.024 W/(m·K). The external surfaces are considered to be grey diffuse bodies having an emissivity and an absorptivity of 0.7.

3.2. Refrigeration plant sizing

The characteristics of the main components of the facility showed in Fig. 1 are collected in Table 4. All the components are sized for a pure CO_2 operating plant, so that if CO_2-HC blends are simulated, a drop-in analysis is performed.

Table 4
Main characteristics of the components the experimental facility consists of.

Component	Parameter	Range
LP Compressor	Swept volume @ 50 Hz	1.88 m^3/h
HP Compressor	Swept volume @ 50 Hz	1.82 m^3/h
	Shaft rotational frequency	30–70 Hz
HP-HX	Height x Width x Depth	360 x 810 x 32 mm
	Number of tubes	20
	Number of rows	2
	Tube diameter	7 mm
	Transverse tube pitch	18 mm
	Longitudinal tube pitch	15.6 mm
	Fin pitch	1.4 mm
	Fin type	Louvered
Evaporator	Height x Width x Depth	360 x 610 x 32 mm
	Number of tubes	20
	Number of rows	2
	Tube diameter	7 mm
	Transverse tube pitch	18 mm
	Longitudinal tube pitch	15.6 mm
	Fin pitch	1.4 mm
	Fin type	Louvered
HP-HX Fan	Model	ebm-papst W3G300-CK13-32
	Nominal rotational speed	1650 rpm
	Nominal flow rate	2300 m^3/h
Evaporator Fan	Model	ebm-papst W3G300-CK13-32
	Nominal rotational speed	1300 rpm
	Nominal flow rate	1650 m^3/h

Table 5
Design operating parameters.

Parameter	Value
Internal air temperature	−18 °C
External air temperature	45 °C
Predicted maximum cooling load	2.1 kW
Design cooling load	3 kW
Design LP compressor superheat	5 K
Design HP-HX pinch-point	2 K

The HP-HX and evaporator are sized in order to satisfy the cooling load at the conditions reported in Table 5. All the components are sized starting from manufacturers' selection software. A fine tuning of FNT HX is done to perfectly match the design parameters. The heat exchangers are built with louvered fins and smooth tubes. The fans are chosen to guarantee at the design conditions a flow rate of ~ 2500 m^3/h at the HP-HX and ~ 1800 m^3/h at the evaporator. Both fans are axial fans operating at fixed speed. On the HP-HX, the air flow related to wind is not considered for the sake of simplicity. Since this work deals with a steady state simulation of the plant, the flash tank volume, which dynamically affects the LP compressor outlet pressure, is not sized. The flash tank pressure, as explained in Section 2 is chosen with an optimizations process.

3.3. Weather data

Temperatures and solar irradiation data are provided on hour basis by CTI (Comitato Termotecnico Italiano (CTI), 2016) at two different Italian locations, namely Milan and Palermo, representative of a temperate and hot European climate. For each hour throughout the year, the temperature of each surface is computed to satisfy Eq. (12) and, with the aim of considering the worst case scenario, the velocity of the truck is set to maximize the heat loss, resulting in a pseudo-still truck (i.e. speed below 1 km/h) during day and in a truck moving at the maximum speed during the night.

4. Results

The simulation campaign covers a comprehensive set of operating conditions, including one representative working point for each

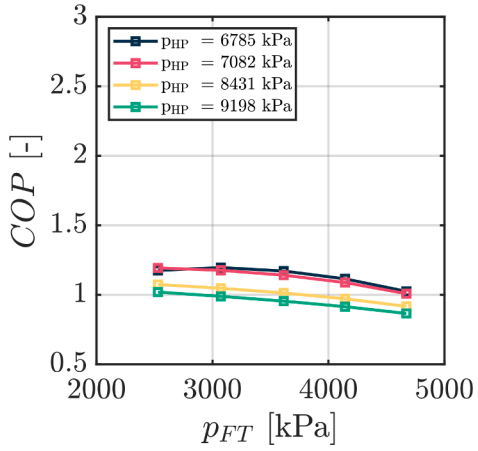

Fig. 5. COP vs p_{FT} for R1270 (8 %) - R744 (92 %) blend at 30 °C at different p_{HP}.

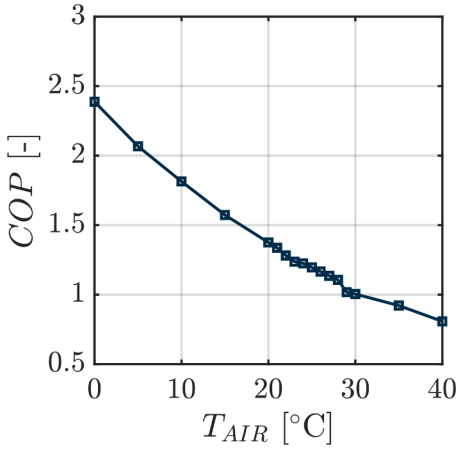

Fig. 6. COP vs T_{AIR} for R1270 (8 %) - R744 (92 %) blend.

combination of refrigerant fluid, mixture composition, and air temperature at HP-HX inlet. For each configuration, simulations were conducted at five distinct flash tank pressures and across four HP-HX pressure levels, resulting in a total of 7140 steady-state operating conditions.

4.1. Results reduction

In this section, all the figures are referred to a single fluid and a single composition in order to create simple yet understandable charts. Specifically, an 8 % Propylene (R1270) - 92 % R744 mixture is chosen as the reference case for plots (T_{CRIT} = 35.72 °C, p_{CRIT} = 7582 kPa). The methodology is then used to include all fluids and all compositions. Simulations are run to compute the COP and, then, the results are further reduced to find the SCOP as per:

$$COP = f(p_{HP}, p_{FT}, T_{AIR}, \text{Fluid type}, y) \tag{18}$$

$$SCOP = f(\text{Fluid type}, y, \text{T distribution}) \tag{19}$$

In each operating mode, the optimal HP-HX pressure p_{HP} and flash tank pressure p_{FT} are found. Indeed, a combination of different p_{HP} and p_{FT} values are considered for each temperature, composition and fluid and then the corresponding COP is computed. Finally, (Eq. 18) is arranged to provide the SCOP (Eq. 19). Fig. 5 shows the COP against p_{FT} at each simulated p_{HP}.

In order to optimize the operating point, the p_{HP} value that maximizes COP for each temperature, composition and fluid is determined by comparing the areas under the COP vs p_{FT} curves computed through trapezoidal integration. With reference to Fig. 5, the chosen p_{HP} that optimizes the system is 6785 kPa. This value corresponds to a subcritical operation, while the other simulated p_{HP} represent transcritical operations.

Once p_{HP} is optimized, p_{FT} is chosen to optimize the system performance. On Fig. 5, a spline curve is interpolated on p_{HP} = 6785 kPa and p_{FT} that gives the optimal working point is chosen as the maximum of this interpolant. With reference to Fig. 5, the optimal p_{FT} is 3020 kPa.

The described process is repeated for each air temperatures at HP-HX inlet and the final result is reported in Fig. 6, in which each point represents the steady state value of COP of the refrigerated truck.

Finally, to find the SCOP value in the different locations, the hour distribution of the ambient temperature, which affects the thermal losses of the truck as described in Section 2.3, is considered. To match the exact value of the external temperature at each hour, the simulation results are linearly interpolated on the temperature. As all the steady state points do not match the required cooling load, the system operates with ON-OFF cycling to match the amount of energy to be extracted from the truck on 1 h basis. Cycling losses due to the dynamic behavior of the system are considered through the formulae proposed in UNI (2022).

The sCOP is then evaluated according to:

$$SCOP = \frac{\sum_{j=1}^{8760} \dot{Q}_C(T_j)}{\sum_{j=1}^{8760} \frac{\dot{Q}_C(T_j)}{EER_{bin}(T_j)}} \tag{20}$$

$$EER_{bin}(T_j) = \frac{\dot{Q}_{EVA}(T_j)}{\dot{W}_{COMP}(T_j)} \cdot \left[1 - 0.25 \cdot \left(1 - \frac{\dot{Q}_C(T_j)}{\dot{Q}_{EVA}(T_j)}\right)\right] \tag{21}$$

4.2. COP behavior with ambient temperature

The behavior of COP with the air temperature at HP-HX inlet at each tested composition is reported in Fig. 7.

Fig. 7 shows that the trend of R1270 mixtures is almost identical to R290 ones while RE170 mixtures behave similarly to R600a ones. The COP reduces with an increase in air temperature, demonstrating the physical adherence of the model to the behaviour of a real system. The higher the ambient temperature, the higher the HP-HX pressure in order to achieve the requested heat rejection. On the other hand, the evaporator pressure does not change that much as it is constrained by the constant air temperature and the fixed superheat, therefore leading to a pressure ratio increase that in turn leads to a efficiency reduction. A sudden slope change is present in the range 20–30 °C in most of the curves, indicating the switch from subcritical to transcritical operation.

For R290 (Fig. 7 (**a**)) and R1270 (Fig. 7 (**c**)) mixtures the COP behavior at all compositions follows the behavior of pure R744. At low air inlet temperatures, the mixtures provide a slightly higher COP (max. + 3.8 % @ T_{AIR} = 0 °C). Indeed, the temperature glide allows for a high-pressure reduction, hence lower compressor work and higher COP. At high air inlet temperatures, the COP is almost identical due to transcritical operation. Here, the mixtures cannot exploit the temperature glide, hence losing their main advantage.

On the other hand, for R600a (Fig. 7 (**b**)) and RE170 (Fig. 7 (**d**)) mixtures, all the curves shift to lower values of COP. For 2 % of R600a and RE170, the behavior is similar to pure R744, but it is clear that the higher the amount of secondary fluid in the mixture, the lower the COP. The degradation is mainly related to the great increase in the total pressure ratio of the cycle, which can raise up to +170 % for 90 % R744 - 10 % R600a, T_{AIR} = 40°C. This phenomenon is a direct consequence of the thermophysical properties of the secondary component (Table 2) as, first, the higher critical temperature and the lower critical pressure induce a higher pressure ratio between the same saturation temperature levels and, then, the higher the glide of the blend, the lower is the LP pressure to allow heat transfer on the evaporator. The COP penalization is lower at low temperatures thanks to the exploitation of the temperature glide, which is not present at high temperatures due to transcritical operation.

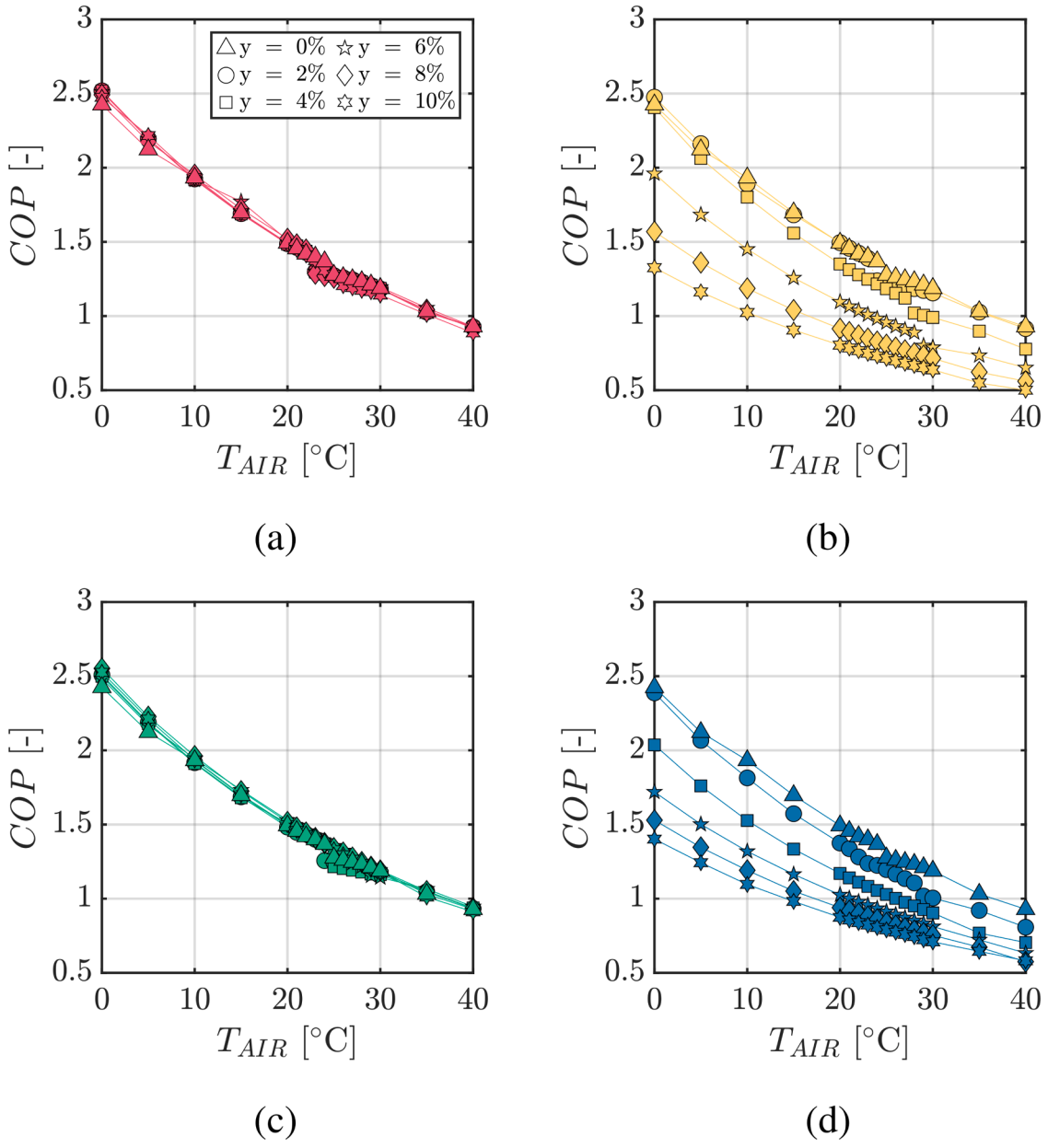

Fig. 7. Behavior of COP against T_{AIR} for (**a**) R290, (**b**) R600a, (**c**) R1270 and (**d**) RE170 mixtures.

4.3. p_{HP} behavior with ambient temperature

The behavior of p_{HP} with the air temperature at gas cooler/condenser inlet at each tested composition is reported in Fig. 8.

For all mixtures, the addition of hydrocarbon reduces the HP-HX pressure with respect to that of R744. This gives an advantage in terms of material saving on tubes and operative parts, i.e., capital cost. Nevertheless, operational cost, which depend on the plant consumption and, consequently, on fuel price, must be accounted for and a trade-off analysis must be performed.

As pointed out previously, the transition temperature for most of the curves from subcritical to transcritical operation is in the range 20–30 °C, as highlighted by the sudden increase in the HP-HX pressure in Fig. 8. It is worth specifying that the lowest transcritical operating pressure, which corresponds to the flat part of the curves in Fig. 8, is much higher than the critical pressure.This is done in order to avoid possible changes from transcritical to subcritical pressure inside the HP-HX due to pressure drop, which in turn generate numerical convergence errors, and to avoid a worse estimation of physical properties near the critical point. The exact location of the temperature at which the transition from subcritical to transcritical operation happens depends on the fluid and the composition. Generally, the higher the amount of hydrocarbon, the higher the critical temperature and the lower the critical pressure and, consequently, the higher the temperature at which the transition happens. This phenomenon leads to an advantage to mixtures instead of pure R744, as there will be a higher range of ambient air working in subcritcal mode.

4.4. $\dot{Q}_{EVA}$ behavior with ambient temperature

The behavior of $\dot{Q}_{EVA}$ with the air temperature at HP-HX inlet at each tested composition is reported in Fig. 9.

The lower density of HCs with respect to R744 significantly reduces the mixture density; since the compressor has a constant swept volume, the mass flow rate is reduced from the baseline case. This phenomenon is the main reason for the reduction of heat transfer by mixtures, as shown

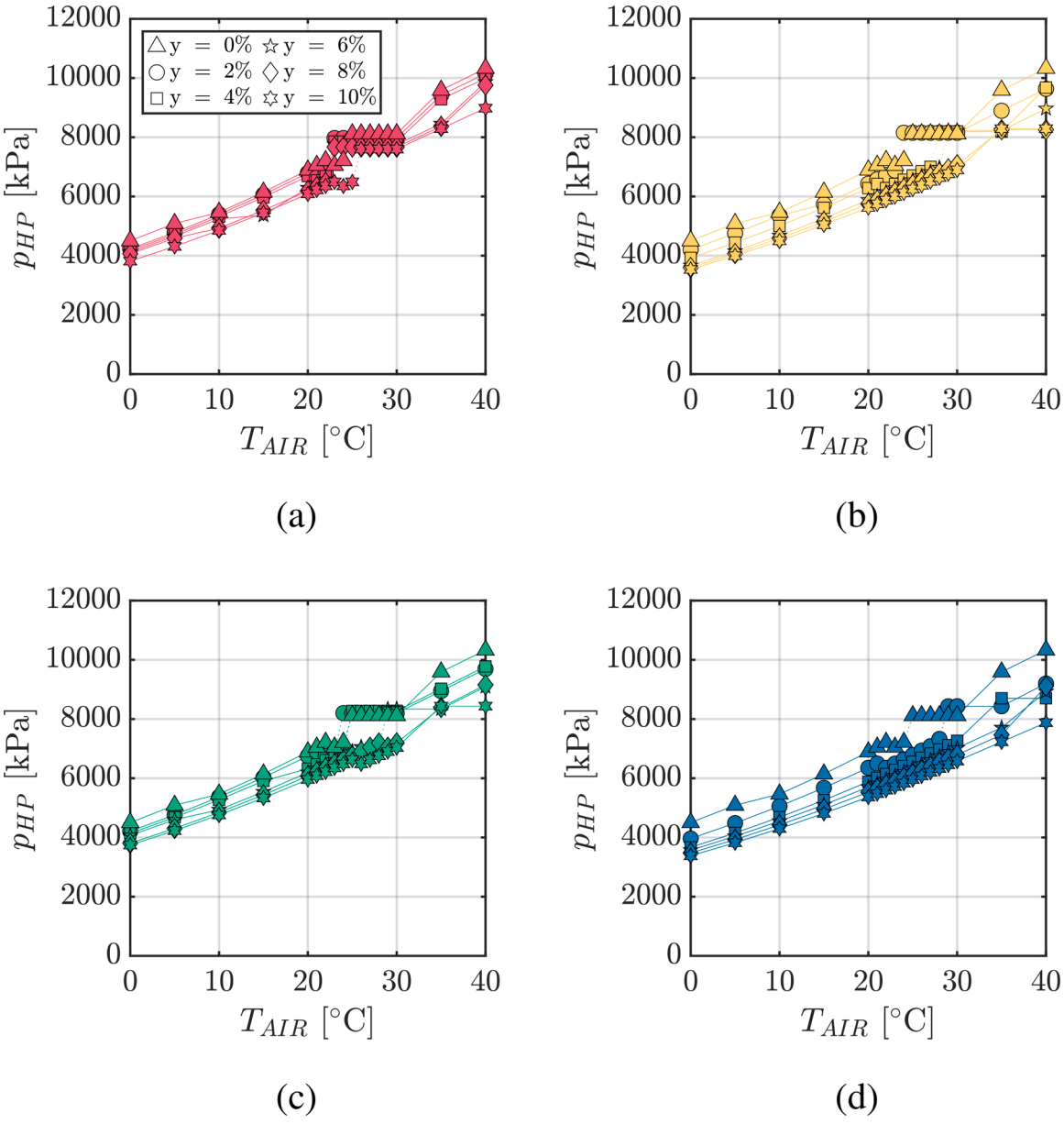

Fig. 8. Behavior of p_{HP} against T_{AIR} for (**a**) R290, (**b**) R600a, (**c**) R1270 and (**d**) RE170 mixtures.

in Fig. 9. The mass flow rate reduction is lower for R290 and R1270 mixtures than for R600a and RE170 mixtures, in view of their higher density (Table 2). Moreover, the mixture glide penalizes heat transfer due to additional mass and heat transfer resistances (Bell and Ghaly, 1972). Consequently, R600a and RE170 mixtures get more penalized than R290 and R1270 mixtures due to the higher glide.

All mixtures show a decreasing trend of heat transfer with the increase in air ambient temperature. Higher air temperature leads to higher HP-HX pressure and flash tank pressure, hence higher vapor quality and lower mass flow rate feeding the evaporator. As the LP compressor is a fixed speed compressor, to provide the required mass flow rate with an increased discharge pressure, the suction pressure (i.e. evaporating pressure) has to increase.This phenomenon increases the compression suction density and, consequently, the mass flow rate, but it reduces the available temperature difference on the evaporator and, consequently, the heat transfer rate. As Fig. 9 suggests, the latter is dominant over the increasing LP mass flow rate. It has to be noted that for R600a and RE170 mixtures the LP mass flow rate stays constant or slightly reduces (according to the composition) since higher air temperatures induce very high LP pressure ratios, hence lower compressor volumetric efficiencies. This phenomenon is less relevant for R290 and R1270 mixtures in view of their lower impact on pressure ratio. Consequently, R600a and RE170 mixtures are more sensitive to an increase in air temperature on $\dot{Q}_{EVA}$.

Above 20 °C ambient temperature, 6 %, 8 % and 10 % mixtures of R744 and either R600a or RE170 cannot satisfy the cooling load in their design points. The HP compressor operates at the maximum allowed frequency; however, the swept volume is still insufficient to handle the required flow rate. Nonetheless, to guarantee the required cooling capacity, a greater swept volume would be necessary. This could be achieved either by adding one or more compressors operating in parallel, by employing a larger compressor, or by increasing the shaft rotational speed. In all cases, the compressors would operate under the same thermodynamic conditions, resulting in comparable isentropic efficiencies and, consequently, similar COP values. Therefore, the same considerations regarding their performance remain valid.

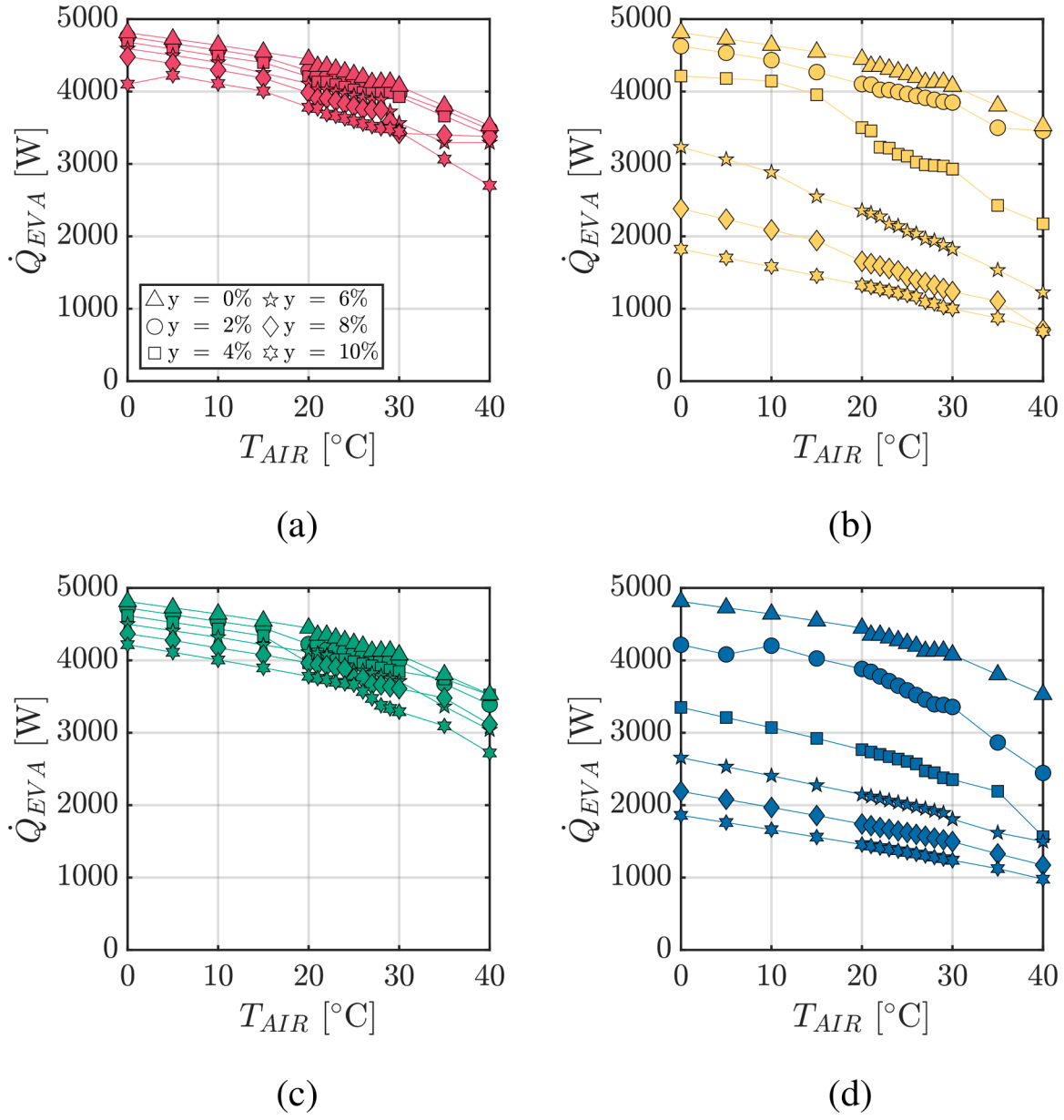

Fig. 9. Behavior of $\dot{Q}_{EVA}$ against T_{AIR} for (**a**) R290, (**b**) R600a, (**c**) R1270 and (**d**) RE170 mixtures.

4.5. $\dot{Q}_{HP}$ behavior with ambient temperature

The behavior of $\dot{Q}_{HP}$ with the air temperature at HP-HX inlet at each tested composition is reported in Fig. 10.

R744, R290 and R600a mixtures exhibit a slightly increasing trend of $\dot{Q}_{HP}$ with ambient temperature up to a threshold value, usually coincident with the switch from subcritical to transcritical operation. Beyond this point, a slightly decreasing trend is observed. Two separate explanations for the two sets of mixtures can be considered.

For pure R744 and its mixtures with R290 and R1270, the mass flow rate below the threshold is almost constant thanks to the action of the inverter driven HP compressor whereas in transcritical operation, the mass flow rate reduces with increasing air temperature as a consequence of the higher pressure ratio. Simultaneously, the higher the HP-HX pressure, the higher the HP-HX inlet temperature and available enthalpy difference. This positive effect is dominant up to the threshold, over which the decrease in mass flow rate overcomes the enthalpy difference increase.

In contrast, R600a and RE170 mixtures face the mass flow rate decrease also in subcritical conditions due to their higher pressure ratio, which penalizes heat $\dot{Q}_{HP}$ through the entire operating range.

4.6. SCOP

The SCOP for pure R744 and the relative deviation for each fluid and composition for the two chosen locations are reported in Table 6.

The use of a mixture composed by R744 and either R1270 or R290 slightly modifies the performance of the system operated with pure R744. A small addition (2 or 4 %) of HC reduces the SCOP value. The induced glide is small, and its benefits are overwhelmed by the reduction in the density and mass flow rate. Nevertheless, there exist optimal compositions for both R1270 (6 %) and R290 (8 %) mixtures that increase the system performance. The most efficient fluid is a mixture of 92 % R744 - 8 % R290, which shows a 2.96 % and 2.13 % increase in SCOP in Milan and Palermo respectively. On the other hand, the use of a mixture

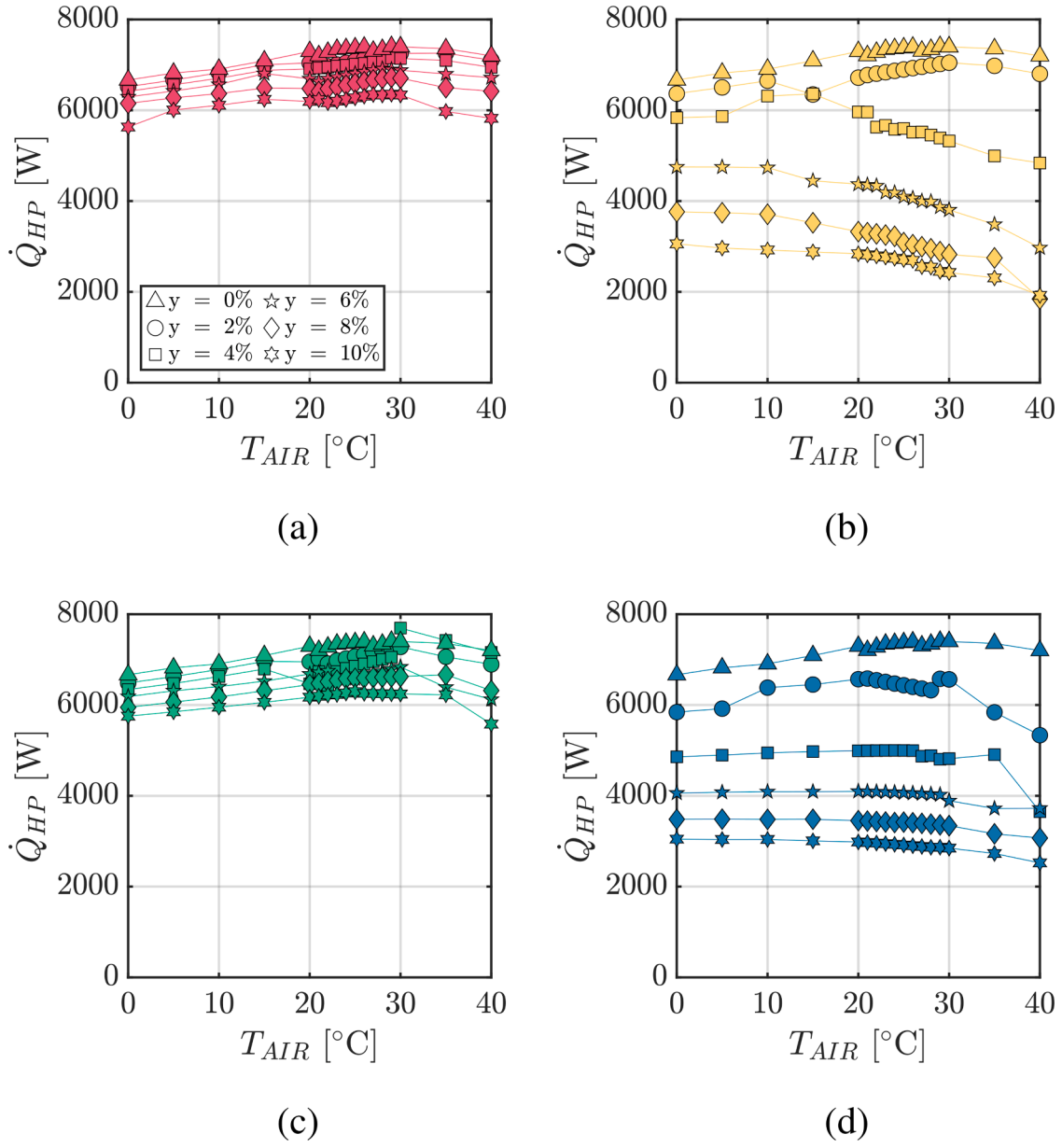

Fig. 10. Behavior of $\dot{Q}_{HP}$ against T_{AIR} for (**a**) R290, (**b**) R600a, (**c**) R1270 and (**d**) RE170 mixtures.

Table 6
SCOP values for the simulated fluids at different compositions considering Milan and Palermo temperature distributions.

SCOP		y											
		0% Milan	2%	4%	6%	8%	10%	0% Palermo	2%	4%	6%	8%	10%
Fluid	R1270-R744	1.69	−0.36 %	−0.30 %	1.24 %	0.59 %	0.24 %	1.536	−0.95 %	−0.77 %	0.83 %	−0.06 %	−0.77 %
	R290-R744	1.69	−0.59 %	−0.41 %	2.19 %	2.96 %	2.01 %	1.536	−1.12 %	−1.12 %	1.54 %	2.13 %	1.18 %
	R600a-R744	1.69	−1.12 %	−8.22 %	−24.85 %	−36.51 %	−43.91 %	1.536	−1.72 %	−8.99 %	−23.85 %	−33.55 %	−39.94 %
	RE170-R744	1.69	−7.34 %	−20.00 %	−29.41 %	−35.15 %	−38.99 %	1.536	−7.99 %	−19.05 %	−26.92 %	−31.83 %	−35.15 %

composed by R744 and either R600a or RE170 drastically reduces the system performance.

Generally, the SCOP values in Palermo are lower than those in Milan due to its hotter climate. This climatic difference also reduces the SCOP improvement achieved by adding R290 or R1270. Specifically, the use of a refrigerant mixture enhances cycle efficiency due to the temperature glide during subcritical operation, which occurs at lower air temperatures . As a result, the system operates more frequently under subcritical conditions in Milan than in Palermo.

Finally, as discussed in Section 4.4, the mixtures provide lower cooling capacity than pure R744, resulting in longer duty cycles and, consequently, reduced cycling losses. While this side effect contributes to an increase in seasonal COP, it should not be interpreted as an intrinsic advantage of the refrigerant mixture. The system was originally designed for pure R744, and the analysis is conducted as a drop-in, i.e., without resizing the components. As a result, the lower density of the mixtures leads to a reduced refrigerant mass flow rate and cooling capacity, which in turn makes the heat exchangers oversized. It is acknowledged

that, if the system were to be resized accordingly, this effect could diminish; however, it would also enable the use of lighter and potentially cheaper components. Such redesign falls outside the scope of this work. Nonetheless, it should be emphasized that the primary contribution to SCOP improvement for mixtures is their more favorable thermodynamic behavior, particularly in subcritical operation, driven by reduced discharge pressures and the exploitation of temperature glide. These aspects are independent of system sizing and constitute the main rationale for further investigation of R744-based mixtures in future studies.

5. Conclusions

An investigation on the performance of a refrigerated truck operating with CO_2 doped with HC is conducted in this study. The goal is to analyze the performance of R744 mixed with small quantities (up to 10 %) of R290, R600a, R1270 and RE170 in a two stage compression refrigeration cycle. A numerical model able to simulate the steady state performance of the plant at different ambient air temperatures is developed. In subcritical mode, the simulations are run with the aim of optimizing the flash tank pressure while in transcritical mode, they are performed to optimize simultaneously the gas cooler and flash tank pressures at the different ambient air temperatures. It is found that mixtures of R744 and R290 or R1270 have similar COP to pure R744 at different temperatures. On the other hand, mixtures of R744 and R600a or RE170 significantly worsen the COP. For all the mixtures, since the compressor swept volume is constant, the heat transfer rate is lower than that of pure R744. For the seasonal COP, two Italian cities, Milan and Palermo, are considered. An optimal composition that enhances the system performance is found at 6 % and 8 % of R1270 and R290 respectively, while R600a and RE170 mixtures always exhibit SCOP decrease. The best performing fluid in this case study is the mixture of 92 % R744 - 8 % R290, which improved the sCOP by 2.96 % and 2.13 % in Milan and Palermo respectively, with colder climates that favor the mixtures with respect to pure R744 thanks to the exploitation of the glide.

Future work will be focused on the experimental validation of the simulation model, mainly on the compressor performance estimation on R744-HCs mixtures. Moreover, an analysis of heat exchangers design and refrigerated truck parameters will be performed to compare the fluids performance under different plant layouts.

CRediT authorship contribution statement

William Ferretto: Writing – original draft, Visualization, Methodology, Data curation, Conceptualization; **Chiara D'Ignazi:** Writing – original draft, Methodology, Formal analysis, Conceptualization; **Igor Matteo Carraretto:** Writing – review & editing, Validation, Supervision, Methodology, Conceptualization; **Luca Molinaroli:** Writing – review & editing, Supervision, Methodology, Funding acquisition, Conceptualization.

Declaration of interest

The authors declare that they have no known competing financial interests or personal relationships that could have appeared to influence the work reported in this paper.

Acknowledgments

The financial support of MIUR through the program PRIN 2022 (Grant Number 20229J4EMW) is greatly acknowledged.

References

Artuso, P., Marinetti, S., Minetto, S., Col, D.D., Rossetti, A., 2020. Modelling the performance of a new cooling unit for refrigerated transport using carbon dioxide as the refrigerant. Int. J. Refrig 115, 158–171. https://doi.org/10.1016/j.ijrefrig.2020.02.032

Bell, K.J., Ghaly, M.A., 1972. An approximate generalized design method for multicomponent/partial condensers. In: AIChE Symp. Ser. Vol. 69, pp. 72–79.

Berdahl, P., Martin, M., 1984. Emissivity of clear skies. Sol. Energy 32, 663–664. https://api.semanticscholar.org/CorpusID:120135716.

Blasius, H., 1913. Das Aehnlichkeitsgesetz bei Reibungsvorgängen in Flüssigkeiten. In: Mitteilungen über Forschungsarbeiten auf dem Gebiete des Ingenieurwesens. Springer Berlin Heidelberg, Berlin, Heidelberg, pp. 1–41. https://doi.org/10.1007/978-3-662-02239-9_1

Calleja-Anta, D., Nebot-Andres, L., Cabello, R., Sánchez, D., Llopis, R., 2022. A3 and a2 refrigerants: border determination and hunt for a2 low-GWP blends. Int. J. Refrig 134, 86–94. https://doi.org/10.1016/j.ijrefrig.2021.11.012

Cao, X., Zhang, C.-L., Zhang, Z.-Y., 2017. Stepped pressure cycle - a new approach to Lorenz cycle. Int. J. Refrig 74, 283–294. https://doi.org/10.1016/j.ijrefrig.2016.10.017

Cavallini, A., Del Col, D., Doretti, L., Matkovic, M., Rossetto, L., Zilio, C., Censi, G., 2006. Condensation in horizontal smooth tubes: a new heat transfer model for heat exchanger design, Heat Transfer Engineering, 27 (8), 31–38. https://doi.org/10.1080/01457630600793970

Comitato Termotecnico Italiano (CTI), 2016. In Italian: Reference metereological year for Italy for HVAC application. Last access on May 22nd 2025. https://try.cti2000.it/page.php?id=1.

Dabiri, A.E., Rice, C.K., 1981. Compressor-simulation model with corrections for the level of suction gas superheat https://www.osti.gov/biblio/6345140.

ESDU, 2014. Design and Performance evaluation of heat exchangers: the effectiveness and NTU method.

E. U. 573/2024, 2024. Regulation (EU) 2024/573 of the European Parliament and of the Council of 7 February 2024 on fluorinated greenhouse gases.

Fabris, F., Artuso, P., Marinetti, S., Minetto, S., Rossetti, A., 2021. Dynamic modelling of a CO2 transport refrigeration unit with multiple configurations. Appl. Therm. Eng. 189, 116749. https://doi.org/10.1016/j.applthermaleng.2021.116749

Fabris, F., Bodys, J., Marinetti, S., Minetto, S., Smołka, J., Rossetti, A., 2024. Numerical modelling of a single-compression multi-temperature ejector-supported R744 refrigeration unit for last mile delivery. Int. J. Refrig. 160, 65–75. https://doi.org/10.1016/j.ijrefrig.2024.01.014

Ferretto, W., Molinaroli, L., Codella, F., 2025. Performance assessment of R-454c, R-449a, and R-744 in food retail refrigeration systems. Energies 18 (3), 667. https://doi.org/10.3390/en18030667

Gnielinski, V., 1976. New equations for heat and mass transfer in turbulent pipe and channel flow. Int. Chem. Eng. 16 (2), 359–368. https://cir.nii.ac.jp/crid/1574231875472963072.bib?lang=ja.

IMARC, 2023. Europe Refrigerated Transport Market Report by Mode of Transportation (Refrigerated Road Transport, Refrigerated Sea Transport, Refrigerated Rail Transport, Refrigerated Air Transport), Technology (Vapor Compression Systems, Air-Blown Evaporators, Eutectic Devices, Cryogenic Systems), Temperature (Single-Temperature, Multi-Temperature), Application (Chilled Food Products, Frozen Food Products, and Others), and Country 2024–2032. https://www.imarcgroup.com/europe-refrigerated-transport-market.

Incropera, F.P., DeWitt, D.P., Bergman, T.L., Lavine, A.S., 2006. Fundamentals of Heat and Mass Transfer. John Wiley & Sons, Hoboken, NJ. 6 ed.

Joppolo, C.M., Molinaroli, L., Pasini, A., 2015. Numerical analysis of the influence of circuit arrangement on a fin-and-tube condenser performance. Case Stud. Therm. Eng. 6, 136–146. https://doi.org/10.1016/j.csite.2015.09.002

Kim, M., 2004. Fundamental process and system design issues in CO2 vapor compression systems. Prog. Energy Combust. Sci. 30 (2), 119–174. https://doi.org/10.1016/j.pecs.2003.09.002

Kim, S.M., Mudawar, I., 2012. Universal approach to predicting two-phase frictional pressure drop for adiabatic and condensing mini/micro-channel flows. Int. J. Heat Mass Transf. 55 (11–12), 3246–3261. https://doi.org/10.1016/j.ijheatmasstransfer.2012.02.047

Kim, S.M., Mudawar, I., 2013. Universal approach to predicting heat transfer coefficient for condensing mini/micro-channel flow. Int. J. Heat Mass Transf. 56 (1–2), 238–250. https://doi.org/10.1016/j.ijheatmasstransfer.2012.09.032

Kondo, S., Takizawa, K., Takahashi, A., Tokuhashi, K., 2006. Extended le chatelier's formula for carbon dioxide dilution effect on flammability limits. J. Hazard. Mater. 138 (1), 1–8. https://doi.org/10.1016/j.jhazmat.2006.05.035

Lemmon, E.W., Bell, I.H., Huber, M.L., McLinden, M.O., 2018. NIST Standard Reference Database 23: Reference Fluid Thermodynamic and Transport Properties-REFPROP, Version 10.0, National Institute of Standards and Technology. https://doi.org/10.18434/T4/1502528

Linteris, G.T., Bell, I.H., McLinden, M.O., 2019. An empirical model for refrigerant flammability based on molecular structure and thermodynamics. Int. J. Refrig. 104, 144–150. https://doi.org/10.1016/j.ijrefrig.2019.05.006

Minetto, S., Fabris, F., Marinetti, S., Rossetti, A., 2023. A review on present and forthcoming opportunities with natural working fluids in transport refrigeration. Int. J. Refrig. 152, 343–355.

Pitla, S.S., Groll, E.A., Ramadhyani, S., 2002. New correlation to predict the heat transfer coefficient during in-tube cooling of turbulent supercritical CO2. Int. J. Refrig. 25 (7), 887–895. https://doi.org/10.1016/S0140-7007(01)00098-6

Reda, I., Andreas, A., 2008. Solar position algorithm for solar radiation applications (revised) https://doi.org/10.2172/15003974

Sánchez, D., Cabello, R., Llopis, R., 2019. Energy improvements in a stand-alone transcritical refrigeration system using a low-GWP mixture of CO2/r1270. https://iifiir.org/dataacite_notices/35195. https://doi.org/10.18462/IIR.ICR.2019.1231

Sánchez, D., Larrondo, R., Vidan-Falomir, F., Cabello, R., 2024. Experimental evaluation of the CO2-based mixtures CO2/R32, CO2/R1234yf and

CO2/R1270 in a transcritical refrigerating plant considering the effect of the internal heat exchanger (IHX). Appl. Therm. Eng. 236, 121473. https://doi.org/10.1016/j.applthermaleng.2023.121473

Sánchez, D., Vidan-Falomir, F., Nebot-Andrés, L., Llopis, R., Cabello, R., 2023. Alternative blends of CO2 for transcritical refrigeration systems. experimental approach and energy analysis. Energy Convers. Manage. 279, 116690. https://doi.org/10.1016/j.enconman.2023.116690

Tobaly, P., Terrier M., F., Boutellier, P., 2018. CO2 + propane mixture as working fluid for refrigeration in hot climates. Experimental results of energy efficiency tests. http://iifiir.org/clientBookline/service/reference.asp?INSTANCE=EXPLOITATION&OUTPUT=PORTAL&DOCID=IFD_REFDOC_0023660&DOCBASE=IFD_REFDOC_EN&SETLANGUAGE=EN. https://doi.org/10.18462/IIR.GL.2018.1276

UNI EN 378-1:2021, 2021. Sistemi di refrigerazione e pompe di calore - Requisiti di sicurezza e ambientali - Parte 1: Requisiti di base, definizioni, criteri di classificazione e selezione.

UNI, E.N., 2022. Air conditioners, liquid chilling packages and heat pumps, with electrically driven compressors, for space heating and cooling - Testing and rating at part load conditions and calculation of seasonal performance.

Vaccaro, G., Milazzo, A., Talluri, L., 2023. Thermodynamic assessment of trans-critical refrigeration systems utilizing CO2-based mixtures. Int. J. Refrig. 147, 61–70. https://doi.org/10.1016/j.ijrefrig.2022.09.013

Wang, C.C., Lee, C.J., Chang, C.T., Lin, S.P., 1999. Heat transfer and friction correlation for compact louvered fin-and-tube heat exchangers. Int. J. Heat Mass Transf. 42 (11), 1945–1956. https://doi.org/10.1016/S0017-9310(98)00302-0

Xie, J., Wang, J., Lyu, Y., Wang, D., Peng, X., Liu, H., Xiang, S., 2021. Numerical investigation on thermodynamic performance of CO2-based mixed refrigerants applied in transcritical system. J Therm Anal Calorim 147 (12), 6883–6892. https://doi.org/10.1007/s10973-021-11011-x

Zhang, M., Webb, R.L., 2001. Correlation of two-phase friction for refrigerants in small-diameter tubes. Exp. Therm Fluid Sci. 25 (3–4), 131–139. https://doi.org/10.1016/S0894-1777(01)00066-8